

PARAMETRIC STUDY OF POWER ABSORPTION PATTERNS INDUCED IN ADULT AND CHILD HEAD MODELS BY SMALL HELICAL ANTENNAS

M. Christopoulou

Biomedical Simulations and Imaging Unit
School of Electrical and Computer Engineering
National Technical University of Athens
Greece

S. Koulouridis

Laboratory of Electrotechnics
Department of Electrical and Computer Engineering
University of Patras
Greece

K. S. Nikita

Biomedical Simulations and Imaging Unit
School of Electrical and Computer Engineering
National Technical University of Athens
Greece

Abstract—A comparative assessment of power absorption in adult and child heads exposed to a small helical antenna at 1710 MHz, is presented, emphasizing the effect of age related parameters. Finite Difference Time Domain simulations are employed to study the interaction between MRI-based head models and a mobile communication terminal equipped with a small helical monopole. A semi-analytical method, based on Green's function theory and the Method of Moments, is used to study the absorption in three-layer spherical head models exposed to a small helical dipole. SAR patterns in child head models derived by non-uniform scaling of adult ones were assessed against SAR patterns computed in child heads derived by uniform downscaling procedures. In both realistic and canonical exposure scenarios, comparable levels of absorbed power

(maximum difference: 12%) in adult and child head models were observed. Dependence of SAR values upon separation distance and tissue dielectric properties was quantitatively assessed. In realistic exposure scenarios, the reduction in peak SAR values was 60–80% for a 1 cm increase in distance and up to 16% for a 110% to 90% decrease in dielectric properties values with reference to the nominal value of 100%. These trends were respectively less (55–65%) and more (up to 24%) emphasized in the corresponding canonical exposure scenarios.

1. INTRODUCTION

All cellular terminals compliance tests require that the induced Specific Absorption Rate (SAR) levels are below the ones recommended by international safety guidelines [1, 2]. Moreover, the worldwide growing rate of mobile phone usage by children, in connection with their developing nervous system and a longer lifetime of exposure [3], requires a precise assessment of the absorbed power by a child's head due to a mobile phone.

In 1996, Gandhi et al. assessed comparatively the SAR values induced in adult and child head models, derived by uniformly scaling down the adult head [4]. They reported a 50% increase in the peak spatial average SAR over 1 g (SAR) induced in the 5 year old child head by a quarter wavelength ($\lambda/4$) monopole antenna mounted on a metal box operating at 835 MHz. In 1998, Schönborn et al. claimed that modeling child head by merely scaling-down adult head may represent an inappropriate approximation [5]. Schönborn et al. used adult and child head models based on magnetic resonance imaging (MRI) scans and found no substantive difference in SAR absorption, due to the near field of linear dipole antennas operating at 900 and 1800 MHz. MRI-based child head models were used in e.g., [6], as well. In 2005, Hadjem et al. computed the power deposition in two realistic child head models, isotropically and anisotropically scaled versions of an adult one, irradiated by a dual-band mobile phone [7]. No important differences were noted in power budget and peak spatial average SAR over 10g (SAR_{10g}) between the adult and the child models.

There is no doubt that numerical results from different research groups may show diverging values due to different preconditions. Even between groups that are nominally using a very similar method for well-defined dosimetric problems, significant differences in computed results can occur [8]. Diversification in the results processing such as normalization to a constant radiated power [4] or to a constant antenna current [5], makes more difficult the direct comparison of the results

between studies [9].

Most of the studies on SAR changes in anatomical human heads, e.g., [4, 5, 9–13] or in spherical head models, e.g., [8, 14] have considered linear antennas as radiating elements. Exposure to helical type mobile phone antennas [15–17] and compliance with SAR limits [15] have been addressed in a limited number of studies.

In this paper, we examine in detail potential age related parameters affecting electromagnetic absorption in anatomical and spherical human head models exposed to small helical antennas, at 1710 MHz. The higher electromagnetic energy density levels induced by the physically shorter helical antenna, as compared to linear antennas [18] and the potentially differing influence of age related parameters on the absorption patterns of the helical antenna have motivated this study.

2. BACKGROUND AND PRESENT WORK

Due to the lack of children MRI data, uniform [4, 16] and non-uniform [7, 9] scaled versions of adult head models are commonly used in literature, to model a child's head. Since the age related developmental changes in the anatomy of various organs follow a quite different course, homogeneous downscaling may not reflect differing growth patterns in the head compared to the rest of the body. Thus, in the present paper, statistical measurement data of head and facial age related parameters [19] have been used to non-uniformly scale the adult head model and derive a 10 year old child head.

The distance between the radiating source and the human head, as well as the intermediate tissue and the ear thickness, are factors that strongly influence the absorbed electromagnetic power. Kuster et al. reported a distribution of slightly compressed ear thickness ranging from 3 to 10 or more mm, with a mean value of about 5 mm [20]. In the present paper, the effect of the age related changes in the elasticity and thickness of the intervening ear is studied by varying the separation distance.

Furthermore, age related variation of the dielectric properties, is certainly an important issue. Comparing younger (10 kg) to older (250 kg) animals, both permittivity and conductivity of almost all tissues were systematically higher for the former ones [21]. For children, according to the approximation proposed in [22], which is based on total body water content, the maximum increase, comparing to adult, in both conductivity and relative permittivity is 15% for a 3 year old child and 8% for a 7 year old child. Hence, in the present paper, we consider a 10 year old boy head model, and we keep the

variation of the dielectric properties values to $\pm 10\%$.

As far as the anatomical, biophysical and biochemical age related changes are concerned, the available literature is quite limited. According to an extensive report [23], the main growth of the brain and head circumference seems to be accomplished in the first 5 years of life. Cranium thickness grows fast during the first decade with concurrent increasing calcification, which results in decreasing conductivity [23], while the temporal bone thickness follows a rapid rate of increase in the first year of life and then a slow steady rate of increase into adulthood [24]. According to the rather poor literature, the age related development of the scalp thickness seems to follow the one of the cranium. Based on these internal anatomy data, a spherical child head model was derived.

3. DESCRIPTION OF EXPOSURE SCENARIOS AND COMPUTATIONAL METHODS

In order to derive an anatomically detailed child head model, a non-uniform downscaling of an MRI-based head model corresponding to a male adult [16, 25] was made, based on statistical measurement data of specific parameters of the head and face of 10 year old boys [19]. The parameters used (Fig. 1) are: the width of the head W , the craniofacial height H_3 , the length of the head L , the height of the lower face H_1 , and the morphological height of the face H_2 . The realistic adult head was segmented, according to facial and head parameters. The segments were scaled down using appropriate scaling parameters. Next, the segments were recomposed and the head model was remeshed into a 1.25 mm grid size, resulting in a non-uniformly scaled (CNU) head model. As the scaling procedure is based on external facial and head anatomy, a detailed check, using in-house developed software [26], assured that none of the internal anatomy tissues was eliminated by the scaling procedure. The dielectric properties of the tissues were based on [27] and were varied for $\pm 10\%$.

Non-uniform scaling was also applied to a three layered spherical adult head illustrated in Fig. 2(b), resulting in a child head model (Child.2). A head radius $a_3 = 7.075$ cm was defined for a 10 year old child, based on an average of male data for head width measurements [19]. Internal anatomy, such as scalp thickness and cranium thickness were defined, according to [24] and are shown in Table 1. The dielectric properties of the tissues are presented in Table 2 and were varied for $\pm 10\%$.

For comparison reasons, the original adult head models (anatomical and spherical) as well as the uniformly downscaled head

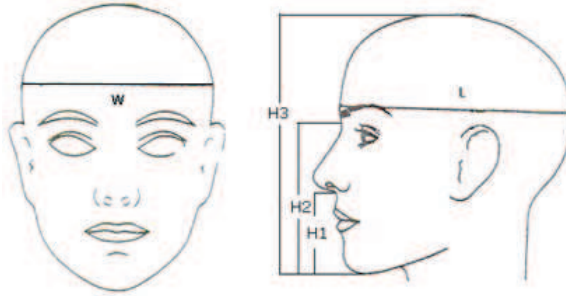


Figure 1. Head and facial parameters used in the non uniform scaling of the adult head model. Modified figure, derived by [19].

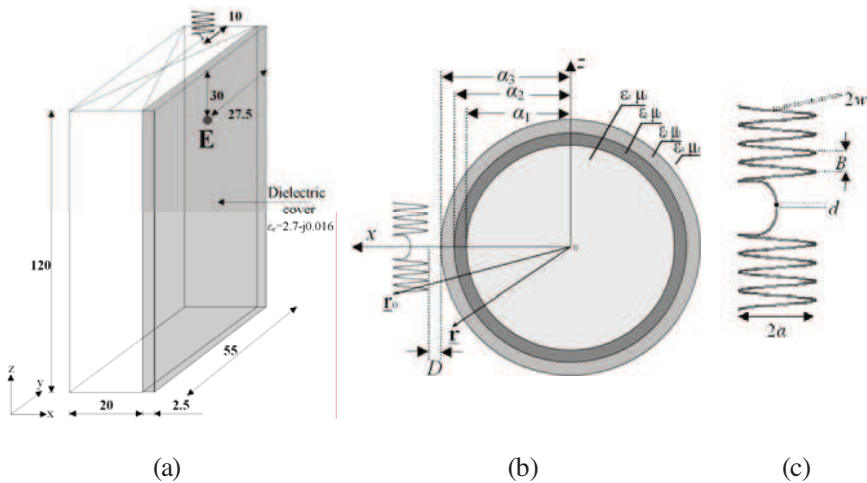


Figure 2. Radiating elements: (a) Handset equipped with a helix monopole used in the FDTD simulations. Dimensions in mm. Point E corresponds to the projection of the ear canal. (b) Geometry of the canonical exposure problem under study. A three-layer spherical head model exposed to the radiation of a helical dipole. Definition of distance D . (c) Detailed geometry of the helical dipole: $\alpha = 2.5$ mm, $B = 1.25$ mm, $w = 0.1$ mm, $L = 4 + 4$ turns, $d = 0.2$ mm. Modified figures, derived by [16].

Table 1. Dimensions of the spherical head models used in canonical exposure problems.

Spherical Head Model	a_1 (cm)	a_2 (cm)	a_3 (cm)
Adult	9.0	9.5	10.0
Child_1 (10 year old)	6.88	7.26	7.64
Child_2 (10 year old)	6.285	6.655	7.075

Table 2. Mass density ρ , conductivity σ and real part of the dielectric permittivity ϵ_r of tissues used in the simulations for canonical exposure problems at 1710 MHz. Simulations for a $\pm 10\%$ variation in the dielectric properties have also been carried out.

Tissue	ρ (kg/m ³)	σ (S/m)	Re(ϵ_r)
Scalp	1100	0.941	38.20
Cranium	1200	0.285	12.00
Brain (grey matter)	1050	1.521	51.80

models (anatomical child: CU and spherical child: Child_1) [16] were also studied. The downscaling procedure was based on height and weight data, changing the dimensions by a factor $\left[\left(\frac{176}{138}\right) \cdot \left(\frac{32.5}{71}\right)\right]^{1/2}$.

As radiating elements, the dielectric covered metal handset box, equipped with a small helical monopole, and the small helical dipole, illustrated in Figs. 2(a), (c) were used, in realistic and canonical exposure scenarios, respectively. The operating frequency is 1710 MHz. The handset used in realistic problems was not designed to provide firm compliance tests but to generically approximate the physical and emission characteristics of a commercial mobile phone. However, the plastic covered box may provide a satisfactory model of the mobile handset, and has been reported to yield SAR_{1g} values within the corresponding ones calculated using CAD files of several commercial mobile phones [28].

Dosimetric simulations for realistic exposure scenarios were based on the Finite Difference Time Domain (FDTD) method (XFDTD[®]1994–2001). A rectangular computational grid, based on the Yee cell, with a spatial resolution of 1.25 mm and the total field formulation have been used, while PML absorbing boundary conditions with 8 PML layers were employed [29]. The boundaries were placed 30 cells away from the nearest scatterer. The total computational grid was constituted by approximately 11.3 million cells (232 × 211 × 231). The interested reader can refer to [16], for details about convergence and accuracy of

FDTD simulations for the small helical antenna.

In order to treat canonical exposure scenarios, a semi-analytical technique, based on the combination of Green's function theory and the Method of Moments (Green/MoM) was used. For a complete mathematical description of the technique and assessment of its accuracy, the interested reader is referred to [16, 30].

Although spherical head models may appear to be rather simplistic compared to the anatomically detailed models, they have been widely used and are still being used in dosimetric studies, e.g., [31, 32]. In this context, Green/MoM technique advantageously provides a means (a) to reproduce the absorption characteristics, being exempt from the uncertainties of the FDTD method, (b) to study the impact of variation of the essential parameters of interest, (c) to easily reveal the relative RF energy source position, (d) to isolate the SAR dependence purely on volume, and (e) to provide a reliable reference to experimental measurements. Additionally, the simulation of the well-defined small helical dipole in the proximity of a spherical head model makes the exposure scenario easily replicable. Through the combined study of realistic and canonical exposure problems, the authors do not intend to obtain directly comparable results, but rather to investigate the feasibility of using canonical exposure scenarios in assessing age related changes in power absorption patterns.

4. NUMERICAL RESULTS

The study of both realistic and canonical exposure problems includes computations of peak local, SAR_{1g} and SAR_{10g} values inside the head, as well as the power absorbed by the head. In realistic exposure scenarios, local SAR values are calculated per each cell. Averaged SAR values over a cubical reference mass $M = 1g$ and $10g$ are calculated according to the averaging method described in [8, 16]. According to this averaging method, the reference mass meets almost the same conditions, comparing to IEEE Std. C95.3-2002. However, no considerations concerning the extremities are taken in account, resulting in higher SAR_{1g}/SAR_{10g} values of approximately 7%, comparing to the ones calculated according to IEEE Std. C95.3-2002. In canonical exposure scenarios, SAR averaging is performed using the procedure described in detail in [16]. All the results presented in Tables 3–6 refer to a total radiated power of 125 mW. The total power radiated from the source, calculated at the feeding point, has been imposed by using the equation $P_i = \text{Re}\{V \cdot I^*\}$, where V and I denote the voltage and the feed point current respectively and $*$ denotes the complex conjugate.

4.1. Variation of the Usage Distance

FDTD simulations for varying separation distance $D' = 0$ mm, 2.5 mm, 5 mm, 7.5 mm, 10 mm between the external ear tissue of the MRI based head models (adult, CU, CNU) and a properly defined point on the front face of the mobile handset, corresponding to the projection of the ear canal (point E , Fig. 2(a)) have been carried out, for a vertically positioned handset.

Table 3. Peak SAR values and absorbed power in anatomically detailed adult and child (CU, CNU) head models exposed to the handset operating at 1710 MHz. The antenna total radiated power is 125 mW. Results produced with FDTD for varying separation distance.

distance D' (mm)	Local SAR (W/kg)			SAR _{1g} (W/kg)		
	Adult	CU	CNU	Adult	CU	CNU
0.0	5.70	5.14	5.84	2.42	2.20	2.32
2.5	3.08	2.76	3.08	1.40	1.69	1.33
5.0	2.21	1.85	2.00	0.95	1.03	1.02
7.5	1.62	1.44	1.41	0.72	0.79	0.68
10.0	1.23	1.14	1.03	0.56	0.62	0.91
distance D' (mm)	SAR _{10g} (W/kg)			Absorbed Power (mW)		
	Adult	CU	CNU	Adult	CU	CNU
0.0	1.35	1.45	1.39	82.81	82.45	79.83
2.5	0.90	1.02	0.86	67.42	67.50	61.72
5.0	0.68	0.70	0.57	55.88	53.98	50.16
7.5	0.49	0.65	0.41	46.91	45.10	41.53
10.0	0.37	0.43	0.31	39.86	38.13	34.88

Table 3 shows the results of FDTD simulations. By comparing the results for the largest separation distance ($D' = 10$ mm) to those for the handset in direct contact with the ear ($D' = 0$ mm), an 82% reduction in the local SAR values is observed for the CNU head and 78% for the adult and CU cases. The reduction in SAR_{10g} is 78% for the CNU model, as compared to 73% and 70% for the adult and CU models, respectively. Irrespective of the distance, local SAR values are generally higher while SAR_{10g} values are lower (4%–37%) in the CNU head than the corresponding ones in CU. Comparing to adult, the SAR_{10g} in CNU is generally smaller (4%–16% depending on the separation distance). As far as the total absorbed power is concerned, 64%, 66% and 66% of the mobile handset input power is absorbed by CNU, adult and CU head models respectively for $D' = 0$ mm. As the separation distance becomes larger ($D' = 10$ mm), the absorbed power

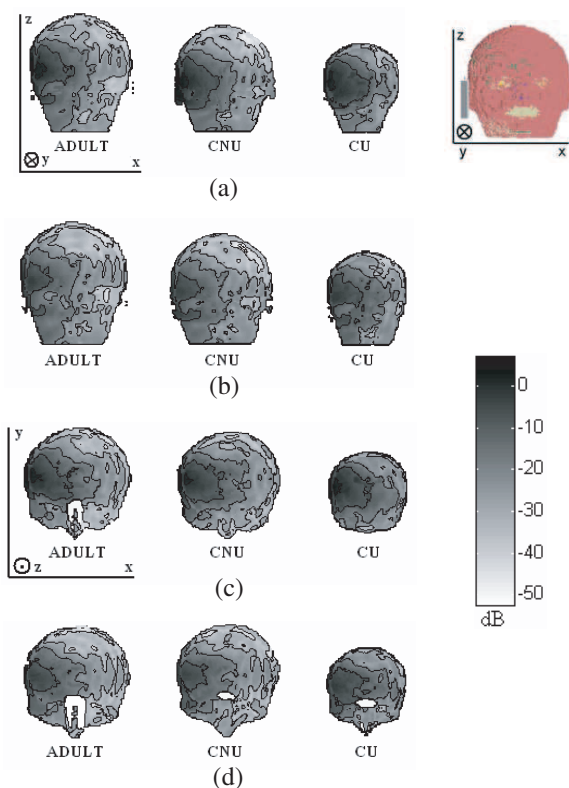


Figure 3. Local SAR distribution, normalized to 1 W/kg in dB for realistic adult and child (CNU and CU) head models in the proximity of a handset equipped with a small helical monopole antenna at 1710 MHz on the xz (a), (b) and xy (c), (d) slices where peak local SAR is calculated. Handset is placed at a distance $D' = 0$ mm (a), (c) and $D' = 10$ mm (b), (d) from the head model.

decreases by factors of 56%, 52%, and 54%, respectively.

In Fig. 3, local SAR distributions, normalized to 1 W/kg, are presented for the slices where the peak local SAR value was calculated, in adult and child head models for $D' = 0$ mm and $D' = 10$ mm. Although the SAR distribution is strongly inhomogeneous, it can be observed that SAR distribution in the CNU is similar to that in the adult head. High SAR regions in the CU head are more extended as compared to those in the adult head, and thus a relatively deeper penetration of absorbed energy is observed in the CU head model. This is consistent with the observation of lower power absorption by the CNU along with its larger size, as compared to the CU. Furthermore, it

Table 4. Peak SAR values and absorbed power in three-layer spherical adult and child (Child_1, Child_2) head models exposed to the helical dipole antenna at 1710 MHz. The antenna total radiated power is 125 mW. Results produced with the Green/MoM technique for varying separation distance.

distance D (mm)	Local SAR (W/kg)			SAR _{1g} (W/kg)		
	Adult	Child_1	Child_2	Adult	Child_1	Child_2
5.0	14.09	13.88	13.88	6.97	7.70	7.86
7.5	11.32	11.36	11.25	5.72	5.91	6.04
10.0	8.95	8.67	8.78	4.49	4.58	4.68
12.5	6.85	6.67	6.66	3.46	3.53	3.59
15.0	5.11	5.06	4.99	2.61	2.69	2.72
distance D (mm)	SAR _{10g} (W/kg)			Absorbed Power (mW)		
	Adult	Child_1	Child_2	Adult	Child_1	Child_2
5.0	3.42	4.41	3.97	117.32	113.00	113.36
7.5	2.91	3.77	3.35	110.07	105.35	105.09
10.0	2.42	3.12	2.75	100.26	95.58	94.84
12.5	1.94	2.52	2.20	88.69	84.96	83.71
15.0	1.53	1.99	1.73	76.76	74.49	72.84

is obvious that as the distance increases, the SAR distribution becomes more uniform.

Simulations for separation distance values $D = 5$ mm, 7.5 mm, 10 mm, 12.5 mm, 15 mm between the spherical head model (adult, Child_1, Child_2) and the helical dipole have been also carried out using the Green/MoM technique. The exact definition of the separation distance D is depicted in Fig. 2(b).

Table 4 shows the results of the Green/MoM simulations. By comparing the results for the largest to those for the closest separation distance, a 64% decrease in the local SAR values can be observed for adult, Child_1, and Child_2 cases. A decrease of 56% (55%) in SAR_{10g} is observed for Child_2 (adult and Child_1). As far as the total absorbed power is considered, 94% (~91%) of the helical dipole input power is absorbed by adult (Child_1 or Child_2) head model for $D = 5$ mm. As the separation distance becomes larger ($D = 15$ mm), the absorbed power decreases by a factor of 35%, 34% and 36% for adult, Child_1 and Child_2, respectively.

Similar to FDTD results, different size spherical head models result in differences in the SAR values and in the power absorbed by the head. The reduction in peak SAR values with increasing separation distance is less pronounced in the canonical exposure scenarios. Comparing the results derived for Child_1 and Child_2 cases,

it can be easily concluded that they present insignificant differences in the peak local SAR values and the total absorbed power. Similarly to anatomical head models results, lower ($\sim 12\%$) $\text{SAR}_{10\text{g}}$ values are observed in Child_2, as compared to Child_1. Additional simulation for a spherical head model with size identical with Child_1 and internal structure (that is skin and bone layer thickness) identical with Child_2 was carried out for the minimum separation distance, resulting in 11% lower $\text{SAR}_{10\text{g}}$, as compared to same size head (Child_1). Moreover, the difference between the $\text{SAR}_{10\text{g}}$ values induced in Child_1 and adult is more emphasized ($\sim 30\%$, for all the distances), than the corresponding one between adult and CU in the realistic exposure scenario (3%–33%, depending on distance).

4.2. Variation of the Head Tissues Dielectric Properties

In order to evaluate the impact of dielectric properties change, separate simulations have been carried out, at the minimum separation distance, for anatomical and spherical head models characterized by dielectric properties with a $\pm 10\%$ variation as compared to the reference values of [27] and Table 2.

The FDTD simulations results are presented in Table 5. By comparing the case of higher to that of lower dielectric properties values, the local SAR values remain unchanged in CNU, and increase

Table 5. Peak SAR values and absorbed power in anatomically detailed adult and child (CU, CNU) head models exposed to the handset operating at 1710 MHz. The antenna total radiated power is 125 mW. Results produced with FDTD for varying dielectric properties, at a separation distance $D' = 0$ mm.

dielectric properties variation as compared to [27]	Local SAR (W/kg)			SAR _{1g} (W/kg)		
	Adult	CU	CNU	Adult	CU	CNU
+10%	5.76	5.42	5.83	2.57	2.29	2.44
0%	5.70	5.14	5.84	2.42	2.20	2.32
-10%	5.48	4.99	5.84	2.23	1.98	2.25
dielectric properties variation as compared to [27]	SAR _{10g} (W/kg)			Absorbed Power (mW)		
	Adult	CU	CNU	Adult	CU	CNU
+10%	1.41	1.53	1.45	81.46	82.41	78.74
0%	1.35	1.45	1.39	82.81	82.45	79.83
-10%	1.30	1.43	1.33	83.73	82.43	80.86

about 5% and 9% in adult and CU head models, respectively. The corresponding increase in SAR_{10g} is of the order of 9%, 8%, and 7%. As far as the total absorbed power is concerned, this becomes slightly lower (3% in adult and CNU) or remains unchanged in CU head, with increasing dielectric properties values.

Table 6. Peak SAR values and absorbed power in three-layer spherical adult and child (Child_1, Child_2) head models exposed to the helical dipole antenna at 1710 MHz. The antenna total radiated power is 125 mW. Results produced with the Green/MoM technique with varying dielectric properties, at a separation distance $D = 5$ mm.

dielectric properties variation as compared to Table 2 values	Local SAR (W/kg)			SAR _{1g} (W/kg)		
	Adult	Child_1	Child_2	Adult	Child_1	Child_2
+10%	14.95	14.86	15.30	8.03	8.34	8.55
0%	14.09	13.88	13.88	6.97	7.70	7.86
-10%	12.43	11.99	12.44	6.64	7.02	7.18
dielectric properties variation as compared to Table 2 values	SAR _{10g} (W/kg)			Absorbed Power (mW)		
	Adult	Child_1	Child_2	Adult	Child_1	Child_2
+10%	3.63	4.69	4.19	117.44	114.10	114.13
0%	3.42	4.41	3.97	117.32	113.00	113.36
-10%	3.20	4.18	3.75	116.53	112.24	112.41

The results of the Green/MoM simulations are shown in Table 6. By comparing the case of higher to that of lower dielectric properties, an increase of 23%, 20%, and 24% in local SAR values is noticed for Child_2, adult, and Child_1, respectively, while the corresponding increase in SAR_{10g} is of the order of 12% for both child head models and 13% for the adult head. As far as the total absorbed power is concerned, an insignificant increase of the order of 1% is observed in adult, and 2% is observed in Child_1 and Child_2.

Additional simulations were carried out for the adult head model at the maximum distance of each scenario for a $\pm 10\%$ variation of the dielectric properties values. By comparing the case of higher to that of lower dielectric properties, for the canonical problem, an increase of 13%, 16% and 9% is observed in peak local SAR, SAR_{1g} and SAR_{10g} values. For the realistic exposure scenario, although there is an increase of 9% and 6% in peak local and SAR_{10g} values, respectively, a 5% decrease is observed in SAR_{1g} values.

5. DISCUSSION

In the present study, a detailed parametric assessment of the power absorption in adult and child head models exposed to small helical antennas at 1710 MHz was presented. The work was devoted to helical antennas and concluded in higher power absorption for the helical type antennas, as compared to linear antennas [18], which has been extensively studied in the literature. The trends in the SAR values as well as in the absorbed power were assessed in realistic and spherical head models, and are summarised in the following:

- a. The exponential decrease of the peak local and SAR_{1g} values induced in realistic and spherical head models with the increase in separation distance, fully agrees with the nature of absorption in near field exposure problems [33, 34]. In spherical head models, the SAR_{10g} values are linearly dependent on the separation distance, since averaging over a larger mass smoothes out the dependence upon distance.
- b. In general, comparable levels (difference less than 5%) of absorbed power were observed in adult and child head models. However, for the maximum separation distance, the power absorbed by the CNU head was up to 12% lower than that absorbed by the adult head.
- c. An increase in SAR values with dielectric properties values increase was observed for the minimum separation distance, which was emphasized more in canonical exposure problems. The power absorbed by the head remained almost constant (differences within 3%). For the realistic exposure scenarios, the age effect of the dielectric properties variation on the SAR_{10g} values did not exceed 9%, which is in agreement with the results of [22]. However, additional simulations, concerning the dielectric properties variation in adult (realistic and spherical) head models for the maximum separation distance, indicated that the trend in SAR variation is also dependent on the anatomy of the exposed region [6], which in turn is related with the relative positioning of the radiating element to the head. In this context, multi-parametric studies involving variation of dielectric properties along with separation distance and varied positioning of the mobile handset should be carried out in order to extend the present study's results.
- d. Comparing the two realistic child head models (CU and CNU), increased local SAR values were calculated for the CNU, while this trend was reversed in SAR_{1g}/SAR_{10g} values. Comparing to

adult, SAR_{10g} values induced in CNU were generally lower (4–16%), depending on the distance. Furthermore, the local SAR values induced in the CU were lower than the corresponding ones in the adult head. This was reversed for SAR_{10g} values, resulting in generally higher SAR_{10g} (3–33%) values induced in CU, as compared to the ones in adult. Differences in variation trends between peak local SAR and SAR_{1g}/SAR_{10g} values are well justified by the averaging procedure, which involves variation in the reference mass composition. The study of the SAR_{1g}/SAR_{10g} values is considered to be more reliable, compared to the local SAR values which are more susceptible to artifacts. In [7], age-related differences in power absorption are also studied for two mobile phones equipped with patch antennas, which concluded in no significant difference in the power budget and SAR_{10g} between child head models derived by uniform and non-uniform downscaling procedures. However, a small difference in SAR values for the brain tissue was reported.

- e. As far as the two spherical child head models are concerned, mild differences (1%–2%) in local and SAR_{1g} values were observed. The SAR_{10g} values calculated in Child_2 were 10–13% lower than their corresponding ones in Child_1, depending on the separation distance. It has to be pointed out that the SAR_{10g} value was strongly related to the internal head structure and specifically to the determination of the center of the 10g cubical mass, in combination with the thickness of the tissue layers. Thus, canonical problems are proven to reveal the effect of uniform vs. non-uniform downscaling, since the observed trends in SAR_{10g} prediction are in agreement with the trends observed in the corresponding realistic scenarios.

The results of the present study were normalized to constant radiated power as this normalization was considered more applicable to practical cases than normalization to constant feed-point current, due to internal power control loop. In this case, the variation on the antenna input impedance might not be so significant for the antenna output power [9, 35, 36]. However, for completeness purposes, the variation of the antenna impedance was studied and the computed values, for $D' = 0$ mm were $6.9 - j8.8$, $6.9 - j8.3$ and $6 - j33.1$ for adult, CNU and CU respectively.

Concluding, in order to address increasing concerns and inquiries regarding age-related exposure assessment, canonical problems are considered to provide worst-case estimation of the power absorption and consistent description of the trends in SAR_{10g} induced values. As far as MRI-based head models are concerned, inter-subject variation

of head size, face and internal anatomy make the derivation of an age-representative child head model quite difficult. Application of literature data concerning age-related thickness of selected tissues may lead to an anatomical child head model for worst-case exposure scenario. However, the use of different adult and child head models is considered statistically safe and crucial for dealing with uncertainty and variation factors [37]. Different electromagnetic sources [38], with varied relative positioning in the proximity of the head should be examined and detailed multi-parametric evaluation of the power absorption patterns should be carried out.

6. CONCLUSION

The objective of the present study was to evaluate the dependence upon age-related parameters of the power absorption and the peak SAR values, induced by a realistic small helical antenna in human head models. The results revealed that comparable power levels (difference lower than 12%) were absorbed by adult and child head models. Assessment of peak SAR values dependence upon separation distance and tissue dielectric properties concluded in a 60–80% decrease for a 1 cm increase in distance and an up to 16% decrease for a 110% to 90% decrease in dielectric properties values with reference to the nominal value of 100% found in [27], for realistic exposure scenarios, depending on the exposed tissue distribution. These trends were respectively less (55–65%) and more (up to 24%) emphasized in the corresponding canonical exposure scenarios. Comparison of the two scaling procedures led to higher (4%–37%) SAR_{10g} values and power absorption values (up to 9%) for the uniformly scaled down head models. These trends were less emphasized (~12% and up to 2%, respectively) in canonical exposure scenarios.

In summary, according to the performed parametric study, trends in SAR values observed in canonical problems were generally in agreement with the ones noticed in realistic exposure scenarios. Thus, canonical problems were proven to be efficient in revealing i) the exponential decrease of the peak local and SAR_{1g} values with the separation distance increase, ii) the general SAR increase with the dielectric properties increase, iii) the effect of the downscaling procedure (uniform vs. non-uniform) on the induced SAR_{10g} values. These observations enhance the power of canonical problems use in low-cost, experimental dosimetry in combination with appropriately designed numerical dosimetric studies.

REFERENCES

1. ICNIRP, "Guidelines for limiting exposure to time-varying electric, magnetic and electromagnetic fields (up 300 GHz)," *Health Phys.*, Vol. 74, 494–522, Apr. 1998.
2. "IEEE standard for safety levels with respect to human exposure to radio frequency electromagnetic fields, 3 kHz to 300 GHz," IEEE, Std C95.1 (Revision of IEEE Std C95.1-1991), 1–238, 2005.
3. *Mobile Phones and Health*, IEGMP, Vol. 15, No. 5, National Radiological Protection Board, Chilton, 2004.
4. Gandhi, O. P., G. Lazzi, and C. M. Furse, "Electromagnetic absorption in the human head and neck for mobile telephones at 835 MHz and 1900 MHz," *IEEE Trans. Microwave. Theory Tech.*, Vol. 44, 1884–1897, Oct. 1996.
5. Schönborn, F., M. Burkhardt, and N. Kuster, "Differences in energy absorption between heads of adults and children in the near field of sources," *Health Phys.*, Vol. 74, 160–168, Feb. 1998.
6. Keshvari, J., R. Keshvari, and S. Lang, "The effect of increase in dielectric values on specific absorption rate (SAR) in eye and head tissues following 900, 1800 and 2450 MHz radio frequency (RF) exposure," *Phys. Med. Biol.*, Vol. 51, 1463–1477, Mar. 2006.
7. Hadjem, A., D. Lautru, C. Dale, M. F. Wong, V. F. Hanna, and J. Wiart, "Study of specific absorption rate (SAR) induced in two child head models and in adult heads using mobile phones," *IEEE Trans. Microwave. Theory Tech.*, Vol. 53, 4–11, Jan. 2005.
8. Nikita, K. S., et al., "A study of uncertainties in modeling antenna performance and power absorption in the head of a cellular phone user," *IEEE Trans. on Microwave Theory Tech.*, Vol. 48, 2676–2685, Dec. 2000.
9. Wang, J. and O. Fujiwara, "Comparison and evaluation of electromagnetic absorption characteristics in realistic human head models of adult and children for 900-MHz mobile telephones," *IEEE Trans. Microwave Theory Tech.*, Vol. 51, 966–971, Mar. 2003.
10. Hirata, A., K. Shirai, and O. Fujiwara, "On averaging mass of SAR correlating with temperature elevation due to a dipole antenna," *Progress In Electromagnetics Research*, PIER 84, 221–237, 2008.
11. Ibrahiem, A., C. Dale, W. Tabbara, and J. Wiart, "Analysis of the temperature increase linked to the power induced by RF source," *Progress In Electromagnetics Research*, PIER 52, 23–46, 2005.
12. Liu, Y., Z. Liang, and Z. Yang, "Computation of electromagnetic

- dosimetry for human body using parallel fdtd algorithm combined with interpolation technique,” *Progress In Electromagnetics Research*, PIER 82, 95–107, 2008.
13. Khalatbari, S., D. Sardari, A. A. Mirzaee, and H. A. Sadafi, “Calculating SAR in two models of the human head exposed to mobile phones radiations at 900 and 1800 MHz,” *PIERS Online*, Vol. 2, No. 1, 104–109, 2006.
 14. Kouveliotis, N. K. and C. N. Capsalis, “Prediction of the SAR level induced in a dielectric sphere by a thin wire dipole antenna,” *Progress In Electromagnetics Research*, PIER 80, 321–336, 2006.
 15. Gandhi, O. P. and G. Kang, “Some present problems and a proposed experimental phantom for SAR compliance testing of cellular telephones at 835 and 1900 MHz,” *Phys. Med. Biol.*, Vol. 47, 1501–1518, Apr. 2002.
 16. Koulouridis, S. and K. S. Nikita, “Study of the coupling between human head and cellular phone helical antennas,” *IEEE Trans. Electromagn. Compat.*, Vol. 46, 62–70, Feb. 2004.
 17. Ebrahimi-Ganjeh, M. A. and A. R. Attari, “Interaction of dual band helical and PIFA handset antennas with human head and hand,” *Progress In Electromagnetics Research*, PIER 77, 225–242, 2007.
 18. Koulouridis, S. and K. S. Nikita, “Characteristics of power absorption in human head models exposed to normal mode helical antennas,” *Proc. Second International Workshop on Biological Effects of Electromagnetic Fields*, Vol. I, 241–250, Rhodes, Greece, Oct. 7–11, 2002.
 19. Farkas, L. G., *Anthropometry of the Head and Face*, 2nd edition, App. A, 244, Raven Press, New York, 1994.
 20. Kuster, N., R. Kästle, and T. Schmid, “Dosimetric evaluation of handheld mobile communications equipment with known precision,” *IEICE Trans. Communications*, Vol. E80-B, 645–652, May 1997.
 21. Peyman, A., S. J. Holden, S. Watts, R. Perrott, and C. Gabriel, “Dielectric properties of porcine cerebrospinal tissues at microwave frequencies: In vivo, in vitro and systematic variation with age,” *Phys. Med. Biol.*, Vol. 52, 2229–2245, 2007.
 22. Wang, J., O. Fujiwara, and S. Watanabe, “Approximation of aging effect on dielectric tissue properties for SAR assessment of mobile telephones,” *IEEE Trans. Electromagn. Compat.*, Vol. 48, 408–413, May 2006.
 23. Reißerweber, J. and J. Poess, “Growth in infancy and

- childhood with tables,” Extensive report supported by FGF, Wireless and Cable Research Group, Department of Information Technology, INTEC, Universiteit Gent, Short-term Mission: Mobile Communication and Children (in the framework of the COST 281 project), Working Group: Anatomical properties and biophysical and biochemical mechanisms, 2003.
24. Simms, D. L. and J. G. Neely, “Thickness of the lateral surface of the temporal bone in children,” *Ann. Oto. Rhinol. Laryn.*, Vol. 98, 726–731, 1989.
 25. Olley, P. and P. S. Excell, “Classification of a high-resolution voxel image of a human head,” *Proc. Int. Workshop at the National Radiological Protection Board*, P. J. Dimbylow (ed.), 16–23, Chilton, U.K., 1995.
 26. Tsakanikas, V. and V. Triantos, “Comparative evaluation of power absorption due to electromagnetic radiation of mobile handsets used by adults and children (FDTD method),” Diploma Thesis (in Greek), NTUA, Jul. 2005.
 27. Gabriel, C., S. Gabriel, and E. Corthout, “The dielectric properties of biological tissues,” *Phys. Med. Biol.*, Vol. 41, 2231–2293, 1996.
 28. Tinniswood, A. D., C. M. Furse, and O. P. Gandhi, “Computations of SAR distributions for two anatomically-based models of the human head using CAD files of commercial telephones and the parallelized FDTD code,” *IEEE Trans. Antennas Propagat.*, Vol. 46, 829–833, Jun. 1998.
 29. Taflov, A. and S. C. Hagness, *Computational Electrodynamics: The Finite-difference Time-domain Method*, 2nd edition, Artech House, 2000.
 30. Koulouridis, S. and K. S. Nikita, “Analysis of the interaction between a layered spherical human head model and an arbitrary shaped antenna using a hybrid Green/MoM technique,” *Proceedings of 8th International Conference on Advances in Communications and Control*, 25–29, Crete, Greece, Jun. 2001.
 31. Mahmoud, K. R., M. El-Adawy, S. M. M. Ibrahim, R. Bansal, and S. H. Zainud-Deen, “Investigating the interaction between a human head and a smart handset for 4G mobile communication systems,” *Progress In Electromagnetics Research C*, Vol. 2, 169–188, 2008.
 32. Kang, X. K., L. W. Li, M. S. Leong, and P. S. Kooi, “A method of moments study of SAR inside spheroidal human head and current distribution along handset wire antennas,” *Journal of Electromagnetic Waves and Applications*, Vol. 15, No. 1, 61–76,

- 2001.
33. Kouveliotis, N. K., S. C. Panagiotou, P. K. Varlamos, and C. N. Capsalis, "Theoretical approach of the interaction between a human head model and a mobile handsets helical antenna using numerical methods," *Progress In Electromagnetics Research*, PIER 65, 309–327, 2006.
 34. Kouveliotis, N. K., P. J. Papakanellos, E. D. Nanou, N. I. Sakka, V. S. G. Tsiafakis, and C. N. Capsalis, "Correlation between SAR, SWR and distance of a mobile terminal antenna in front of a experimental validation," *Journal of Electromagnetic Waves and Applications*, Vol. 17, No. 11, 1561–1581, 2003.
 35. Yoshida, K., A. Hirata, Z. Kawasaki, and T. Shiozawa, "Human head modeling for modeling for handset antenna design at 5 GHz band," *Journal of Electromagnetic Waves and Applications*, Vol. 19, No. 3, 401–411, 2005.
 36. Kiminami, K., A. Hirata, Y. Horii, and T. Shiozawa, "A study on human body modeling for the mobile terminal antenna design at 400MHz band," *Journal of Electromagnetic Waves and Applications*, Vol. 19, No. 5, 671–687, 2005.
 37. Kainz, W., A. Christ, T. Kellom, S. Seidman, N. Nikoloski, B. B. Beard, and N. Kuster, "Dosimetric comparison of the specific anthropomorphic mannequin (SAM) to 14 anatomical head models using a novel definition for the mobile phone positioning," *Phys. Med. Biol.*, Vol. 50, 3423–3445, Jul. 2005.
 38. Li, L. W., M. S. Leong, P. S. Kooi, and T. S. Yeo, "Specific absorption rates in human head due to handset antennas: A comparative study using FDTD method," *Journal of Electromagnetic Waves and Applications*, Vol. 14, No. 7, 987–1001, 2000.